Geoscience Frontiers 12 (2021) 1018–1030

HOSTED BY

Contents lists available at ScienceDirect

Geoscience Frontiers

journal homepage: www.elsevier.com/locate/gsf

Research Paper

Raman and infrared spectroscopic quantification of the carbonate concentration in K_2CO_3 aqueous solutions with water as an internal standard

Yunlu Ma [a,b], Wei Yan [a,b], Qiang Sun [a,b], Xi Liu [a,b,*]

[a] School of Earth and Space Sciences, Peking University, Beijing 100871, China
[b] Key Laboratory of Orogenic Belts and Crustal Evolution, Ministry of Education of China, Beijing 100871, China

ARTICLE INFO

Keywords:
Carbonate aqueous solution
Micro fluid inclusion
K_2CO_3 concentration
Relative Raman intensity
Relative IR absorbance

ABSTRACT

Carbonate-bearing fluids widely exist in different geological settings, and play important roles in transporting some elements such as the rare earth elements. They may be trapped as large or small fluid inclusions (with the size down to <1 μm sometimes), and record critical physical-chemical signals for the formations of their host minerals. Spectroscopic methods like Raman spectroscopy and infrared spectroscopy have been proposed as effective methods to quantify the carbonate concentrations of these fluid inclusions. Although they have some great technical advantages over the conventional microthermometry method, there are still some technical difficulties to overcome before they can be routinely used to solve relevant geological problems. The typical limitations include their interlaboratory difference and poor performance on micro fluid inclusions. This study prepared standard ion-distilled water and K_2CO_3 aqueous solutions at different molarities (from 0.5 to 5.5 mol/L), measured densities, collected Raman and infrared spectra, and explored correlations between the K_2CO_3 molarity and the spectroscopic features at ambient *P-T* conditions. The result confirms that the Raman O–H stretching mode can be used as an internal standard to determine the carbonate concentrations despite some significant differences among the correlations, established in different laboratories, between the relative Raman intensity of the C–O symmetric stretching mode and that of the O–H stretching mode. It further reveals that the interlaboratory difference can be readily removed by performing one high-quality calibration experiment, provided that later quantifying analyses are conducted using the same Raman spectrometer with the same analytical conditions. Our infrared absorption data were collected from thin fluid films (thickness less than ~2 μm) formed by pressing the prepared solutions in a Microcompression Cell with two diamond-II plates. The data show that both the O–H stretching mode and the O–H bending mode can be used as internal standards to determine the carbonate concentrations. Since the IR signals of the C–O antisymmetric stretching vibration of the CO_3^{2-} ion, and the O–H stretching and bending vibrations from our thin films are very strong, their relative IR absorbance intensity, if well calibrated, can be used to investigate the micron-sized carbonate-bearing aqueous fluid inclusions. This study establishes the first calibration of this kind, which may have some applications. Additionally, our spectroscopic data suggest that as the K_2CO_3 concentration increases the aqueous solution forms more large water molecule clusters via more intense hydrogen-bonding. This process may significantly alter the physical and chemical behavior of the fluids.

1. Introduction

Carbonate aqueous solutions widely exist in the Earth's crust and upper mantle, and have great contributions in transporting rare earth elements and other elements (Roedder, 1984). Carbonate-bearing fluids may appear in the deep lithosphere and potentially be responsible for the formation of diamonds via some mechanisms such as reduction and/or cooling (e.g., Deines, 1980; Tomlinson et al., 2009; Stagno and Frost, 2010; Aulbach et al., 2011; Luth and Stachel, 2014; Tao et al., 2015; Smart et al., 2017). When trapped as inclusions in minerals, these

* Corresponding author. School of Earth and Space Sciences, Peking University, Beijing 100871, China.
E-mail address: Xi.Liu@pku.edu.cn (X. Liu).
Peer-review under responsibility of China University of Geosciences (Beijing).

https://doi.org/10.1016/j.gsf.2020.03.002
Received 11 October 2019; Received in revised form 1 January 2020; Accepted 9 March 2020
Available online 13 March 2020

carbonate-rich fluids may partially crystallize to form some carbon polytypes (e.g., graphite and diamond; Zhu and Ogasawara, 2002) or carbon-bearing minerals (e.g., nahcolite; Bühn et al., 2002), which should contain valuable information related to the compositions of the fluids, and the physical and chemical environment conditions such as temperature (*T*), pressure (*P*), and host rock chemistry (e.g., Izraeli et al., 2001; Yamamoto et al., 2002; Tomlinson et al., 2006; Kopylova et al., 2010; Thomas et al., 2011). Consequently, quantitative analyses of the carbonate-bearing fluid inclusions have great applications in interpreting water-rock interaction and rock-forming processes, searching for ore deposits, and exploring fluid supercritical phenomena (e.g., Bakker and Mamtani, 2000; Wilkinson, 2001; Roedder, 2003).

There have been many investigations on the fluid inclusions, with the effort mainly devoted to the large ones (e.g., diameters ranging from ~5 to 50 μm; Frezzotti et al., 2012) due to some limitations of the commonly used analyzing methods. The much smaller fluid inclusions (<1 μm), or micro fluid inclusions, as those found in some fibrous diamonds in many places, may contain different but certainly significant information (e.g., Kamiya and Lang, 1965; Navon et al., 1988; Schrauder and Navon, 1994), and should be similarly investigated. In these cases, a quantifying method should be of high value.

The most used conventional analytical method for small fluid inclusions, the microthermometry method, has some limitations. It measures the final melting point of the fluid inclusion by heating the frozen sample, and then determines the salinity of the solution by resorting to appropriate phase diagrams (Roedder, 1984). This method has some technical difficulties in acquiring an accurate result due to possible inclusion stretching during the frozen process, clathrate formation and/or metastable state (Yamamoto et al., 2002; Kagi et al., 2006). It may be inapplicable to the fluid inclusions in opaque minerals, or the micro fluid inclusions, where clear visual observation of the contents of the inclusions is very difficult. In addition, the correspondingly required phase diagrams may be not always available. Some other conventional methods need to crack the fluid inclusions, which may potentially introduce some contaminants or lead to loss of the volatiles (Sun and Zeng, 2000).

Newly developed analytical methods for the fluid inclusions include spectroscopic methods. Raman spectroscopy has proved to be a great in situ, non-destructive, and non-contact method to perform qualitative and quantitative analyses on the fluid inclusions (e.g., Frezzotti et al., 2012; Wang et al., 2013). Moreover, it provides a light spot as small as ~1 μm, which allows the spectroscopic analyses to be performed on the micro fluid inclusions (Pasteris et al., 1988). It has been employed to investigate the carbonate concentrations, CO_3^{2-}-HCO_3^- equilibrium, and hydrogen-bond components in the carbonate aqueous solutions, which significantly deepens our understanding on these solutions (e.g., Oliver and Davis, 1973; Rudolph et al., 2006; 2008; Wu and Zheng, 2010; Sun and Qin, 2011). However, this method has some disadvantages. Raman scattering from the water-rich carbonate-bearing fluids may be very weak. Potentially strong luminescence from some host minerals may block out the weak Raman signals and thus impair the measurement. It is usually hard to precisely focus the laser beam on the micro fluid inclusions. More importantly, different analytical conditions or experimental setups may result in significant differences in the Raman scattering intensities which are used to quantify the corresponding components. Extensive, and cumbersome, calibration for different Raman systems in different laboratories hence becomes a prerequisite for any accuracy measurements.

Fourier transform infrared spectroscopy (abbreviated as IR hereafter) is generally a complementary tool to Raman spectroscopy, and has been employed in some fluid inclusion studies as well. Many IR investigations have been conducted to study the structures of the carbonate aqueous solutions (e.g., Oliver and Davis, 1973; Rudolph et al., 2006). Yet, a systematic IR calibration of the carbonate concentrations in aqueous solutions has not been fully reported. Kagi et al. (2006) established some correlation curves between the salinities of some standard salt aqueous solutions and the antisymmetric stretching + bending combination IR band of water (~5180 cm^{-1}). However, this combination band is very weak, which requires the fluid inclusions to be very large or densely populated in order to obtain a meaningful absorbance (larger than ~30 μm; Kagi et al., 2006) and accordingly requires the mineral sample to be very thick. Firstly, large fluid inclusions are not always available, and micro fluid inclusions may sparsely appear only. Secondly, the long infrared light pathway may be not entirely clear, resulting in high risks in the analyses with IR signals from other materials rather than from the fluid inclusions only. Additionally, the weak signal of the combination IR band of water at ~5180 cm^{-1} means that a large number of scans are required in order to reach a good signal-to-noise ratio. In comparison, the fundamental O–H vibration modes have much higher absorption, and should be more suitable for quantitative analyses on the micro fluid inclusions.

In this study, we prepared ion-distilled water and K_2CO_3 aqueous solutions at different molarities (from 0.5 to 5.5 mol/L), measured their densities, collected their unpolarized Raman spectra and IR spectra at ambient *P-T* conditions (1 atm and 27 °C). By comparing our relative Raman intensity data with others, we explored some aspects of the Raman quantification factor (*F*) of these aqueous solutions. The result may facilitate future interlaboratory comparison, and simplify the Raman spectroscopic measurements on the fluid inclusions. We also determined the correlation between the CO_3^{2-} concentration of the carbonate aqueous solutions with the relative IR absorbance of the fundamental C–O antisymmetric stretching mode (IR peak at ~1400 cm^{-1}) and fundamental O–H stretching vibration mode (broad IR peak at ~3417 cm^{-1}) or O–H bending vibration mode (IR peak at ~1655 cm^{-1}). This calibration should find itself some applications in quantifying the sparsely-populated carbonate-rich micro fluid inclusions.

2. Experimental methods

Preparation of solutions. The K_2CO_3 aqueous solutions were prepared at different K_2CO_3 molarities (mol/L). Analytical grade K_2CO_3 powder ($K_2CO_3 \geq 99.0\%$) was dried at 450 °C for 20 h, cooled to room *T*, immediately weighted, and then dissolved in ion-distilled water held in beakers. Volumetric flasks with capacities of 25, 50, and 100 mL were used for controlling the final volumes. The final solutions were immediately sealed in airtight bottles after the preparation.

The densities of these solutions were measured using a graduated cylinder (10 mL volume) at room temperature (27 (2) °C). This experimental method was verified by our multiple measurements performed on the ion-distilled water, which yielded a density of 0.9973 (99) g/mL (8 measurements).

Raman spectroscopic measurements. The unpolarized Raman spectra of our ion-distilled water and K_2CO_3 aqueous solutions, from 100 to 4500 cm^{-1}, were recorded at ambient *P-T* conditions. A confocal micro-Raman system (Renishaw inVia Reflex system; Lu et al., 2019) was used in our experiments. The measurements were performed in a back-scattering geometry, with other experimental conditions as following: a 532 nm laser, an emission power of 50 mW, a light spot of ~1 μm, a 50× objective and an entrance slit of 65 μm. Every spectrum was recorded using a 5 s counting time, one accumulation, and a resolution of ±1 cm^{-1}. The Raman spectra were processed by the Peakfit v4.12 software (the AutoFit Peaks I Residuals option).

Infrared spectroscopic measurements. The ambient unpolarized IR spectra, from 675 to 7800 cm^{-1}, were recorded using a Nicolet iN10 MX IR Microscope coupled with a Microcompression Cell with two diamond-II plates (Fig. 1). This IR microscope was equipped with a high-energy Ever-Glo™ infrared source, a KBr beam splitter, and a liquid-nitrogen-cooled MCT detector (Liu et al., 2017; He et al., 2019). The transmission IR spectra were collected with an aperture size of 50 × 50 μm^2, 64 scans, and a resolution of 4 cm^{-1}.

For each experiment, one droplet of the ion-distilled water or K_2CO_3 aqueous solutions (~0.050 (5) mL) was loaded on one of the two diamond plates (~2 mm in diameter, ~1 mm in thickness, Fig. 1), gently

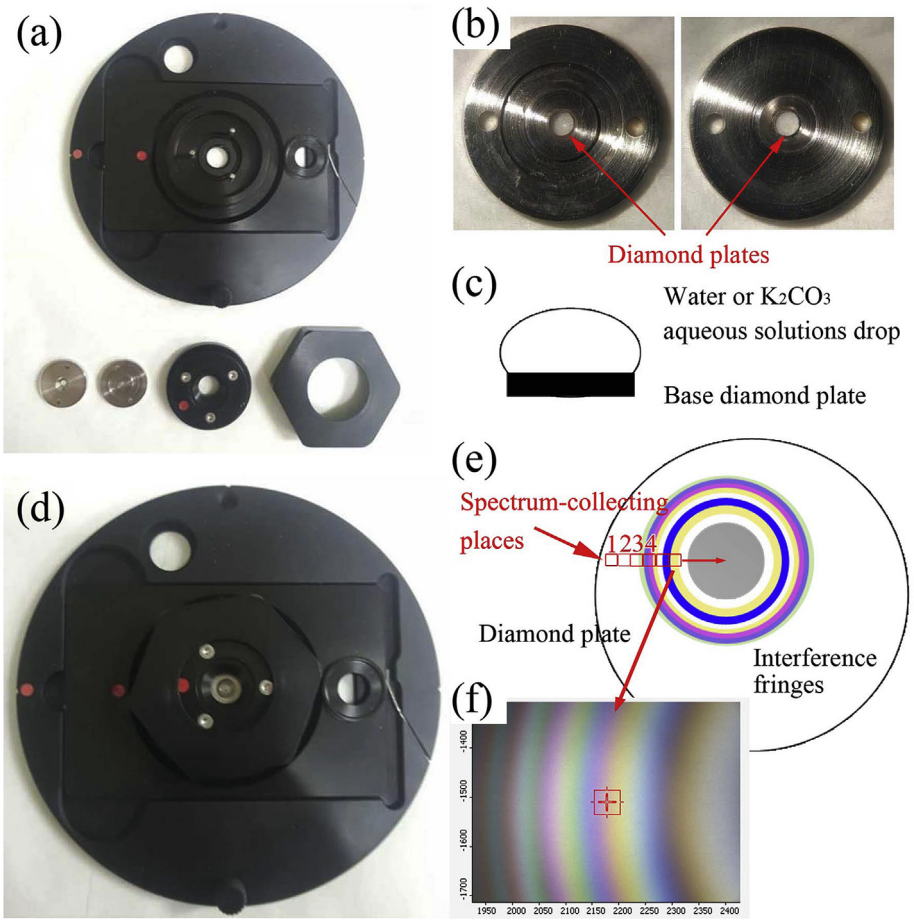

Fig. 1. Microcompression Cell with windows made of two diamond-II plates for IR measurements: (a) the components, (b) enlargement of the window, (c) sketch of the base diamond plate with one droplet of solution, (d) the fully assembled cell, (e) sketch of the pseudo-Newton's rings in the Microcompression Cell loaded with a solution sample (spectrum-collecting positions marked by red open squares), (f) typical photo of the pseudo-Newton's rings (see text for more details).

pressed by the other to form a thin film (no gasket used), and then probed by the IR beam. The background of the IR experiment was collected with no sample loaded between the two diamond plates.

As the sample droplet was pressed between the two diamond plates, a wedged thin film formed due to the slight deformation of the diamond plates caused by the uniaxial compression. Pseudo-Newton's rings were then developed (Fig. 1). The center of the pseudo-Newton's rings usually did not appear at the center of the surface of the round diamond plates, indicating that the pressing was not completely even. These pseudo-Newton's rings were very useful in our experiments for they could be conveniently used to define the thickness trend of the liquid film, with the thickness gradually increasing from the center position to the rim position. In every experiment, the rim position of the pseudo-Newton's rings was probed by the IR beam, and the amount of compression exerted on the diamond plates was accordingly adjusted. Eventually a suitable sample thickness at the rim position was found, with the absorption of the major IR signals ranging from ~0.7 to 1.0 unit. The possibility of the non-linear detector response errors in the IR analyses was then minimized, leading to a better accuracy in our IR data (King et al., 2004).

This study aimed at the *P* condition of 1 atm, so that all the IR spectra reported for our solutions were collected from the rim positions of the pseudo-Newton's rings, where the liquid samples had finite thickness and the pressure was equal to the room *P*. Anyhow, no pressure gradient was expected to occur in the solutions. In the experiment with the pure water we nevertheless collected a series of IR spectra, from the rim position towards the center position of the pseudo-Newton's rings. No pressure gradient was found out indeed (see later discussion).

All our IR spectra were processed by the Peakfit v4.12 software (the AutoFit Peaks I Residuals option).

3. Results and discussions

3.1. Densities of water and K_2CO_3 aqueous solutions

The densities of our water and K_2CO_3 aqueous solutions are listed in Table 1, and shown in Fig. 2. As expected, the density increases as the K_2CO_3 molarity (*c*; mol/L) increases. For the purpose of comparison, Fig. 2 also shows the data obtained at a slightly lower *T* from Söhnel and Novotny (1985; 20 °C), which are much compatible with our results at 27 °C.

3.2. Raman features of K_2CO_3 aqueous solutions and quantification

According to the group theory, the CO_3^{2-} ion has the symmetry D_{3h} and attains four fundamental vibrational modes: the C–O symmetric stretching mode at ~1060 cm^{-1} (Raman-active only), the out-of-plane deformation mode at ~884 cm^{-1} (infrared-active only), the C–O anti-symmetric stretching mode at ~1395 cm^{-1} (both Raman-active and infrared-active), and the in-plane deformation mode at ~684 cm^{-1} (both Raman-active and infrared-active). In most SiO_2-bearing geological fluids, the Raman peak at ~684 cm^{-1} is not only weak, but also may be severely affected by the strong Raman signals of the SiO_4 structural units. The Raman peak at ~1395 cm^{-1} is also not very strong. In contrast, the C–O symmetric stretching mode at ~1060 cm^{-1} is often strong and least affected by most other species in the fluids, and thus superbly useful in

Table 1
Density and Raman features of water and K_2CO_3 aqueous solutions.

			CO_3^{2-}			H_2O		CO_3^{2-}/H_2O	
c (mol/L)	ρ(g/mL)	c (CO_3^{2-})/c(H_2O)[a]	Center[b]	I_{Height}	I_{Area} (cm^{-1})	I_{Height}[c]	I_{Area} (cm^{-1})[c]	*R.I.* (Height)	*R.I.* (Area)
0.00 (0)[d]	1.00 (1)[e]	0.000 (0)				20,478 (8010)	3,971,414 (1,340,382)		
0.50 (2)	1.06 (1)	0.009 (1)	1066.34 (5)	2503 (27)	35,159 (428)	24,816 (5499)	5,451,342 (1,527,710)	0.10 (2)	0.006 (2)
1.00 (3)	1.11 (1)	0.019 (1)	1066.11 (3)	3946 (25)	54,183 (423)	18,542 (1616)	4,298,026 (764,676)	0.21 (2)	0.013 (2)
1.50 (5)	1.16 (1)	0.028 (2)	1065.79 (2)	6205 (24)	84,310 (408)	19,455 (2406)	4,491,653 (542,871)	0.32 (4)	0.019 (2)
2.00 (6)	1.21 (1)	0.038 (3)	1065.49 (2)	9920 (41)	133,450 (631)	22,573 (4587)	5,279,186 (635,960)	0.44 (9)	0.025 (3)
2.50 (8)	1.26 (2)	0.049 (4)	1065.24 (2)	9839 (35)	135,240 (560)	16,684 (11051)	4,121,429 (1,709,416)	0.59 (39)	0.033 (14)
3.00 (9)	1.30 (1)	0.061 (5)	1064.88 (2)	12,403 (42)	171,520 (682)	17,589 (3754)	4,343,738 (556,148)	0.71 (15)	0.039 (5)
3.50 (11)	1.35 (2)	0.073 (6)	1064.57 (2)	8549 (27)	120,460 (494)	9581 (2034)	2,518,721 (2,266,761)	0.89 (19)	0.048 (43)
4.00 (12)	1.38 (1)	0.087 (7)	1064.22 (1)	11,106 (33)	157,840 (603)	11,124 (1722)	2,872,127 (1,073,189)	1.00 (16)	0.055 (21)
4.50 (14)	1.43 (1)	0.100 (8)	1063.86 (2)	9228 (31)	134,200 (602)	8225 (5521)	2,154,776 (865,215)	1.12 (76)	0.062 (25)
5.00 (15)	1.46 (1)	0.117 (10)	1063.48 (1)	16,522 (39)	243,150 (796)	13,032 (4878)	3,449,765 (871,197)	1.27 (48)	0.070 (18)
5.50 (17)	1.52 (2)	0.131 (12)	1063.14 (1)	26,812 (69)	396,330 (1424)	18,278 (10711)	4,884,562 (969,987)	1.47 (86)	0.081 (16)

[a] This refers to the relative concentration of the CO_3^{2-} ion (mol/L) to the H_2O (mol/L) calculated according to the measured density.
[b] Center refers to the peak position of the CO_3^{2-} in cm^{-1}.
[c] The intensity and area of the water peak were derived by summing up the intensity and area of the five band components, respectively.
[d] Number in parentheses is one standard deviation in the rightmost digit. The concentration errors of the K_2CO_3 aqueous solutions are assumed as 3%.
[e] Densities of our K_2CO_3 aqueous solutions were determined by averaging 8 measurement data for each sample.

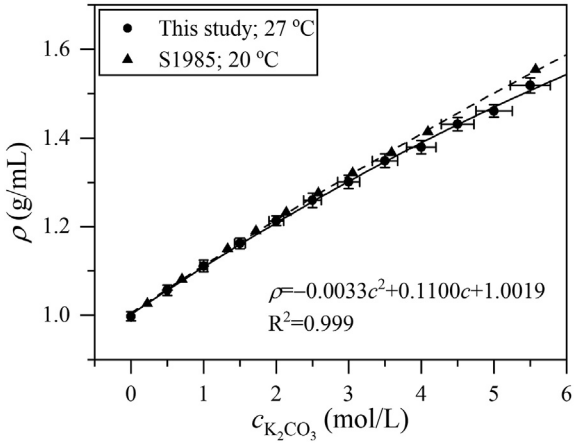

Fig. 2. Density versus K_2CO_3 molarity ($c_{K_2CO_3}$ in mol/L) of the prepared aqueous solutions. The uncertainty of the $c_{K_2CO_3}$ has been assumed as 3%. S1985, Söhnel and Novotny (1985). The solid curve is for the data at 27 °C from this study, and the dashed curve is for the data at 20 °C from the literature. The effect of T on the density of the K_2CO_3 aqueous solutions seemingly increases with the $c_{K_2CO_3}$ increases.

quantifying the CO_3^{2-} ion concentration. We consequently have chosen this vibration mode to make our discussions.

3.2.1. *Fitting the Raman spectra*

The Raman spectra of our ion-distilled water and K_2CO_3 aqueous solutions at different molarities are shown in Fig. 3. Clearly, the Raman peak at ~1060 cm^{-1} for the CO_3^{2-} ion in the K_2CO_3 aqueous solutions is sharp, with its intensity positively correlating with the CO_3^{2-} ion concentration. In contrast, the Raman peak for the solvent water is very broad, ranging from ~3000 to 3700 cm^{-1} (e.g., Walrafen, 1964; Perchard, 2001; hereafter denoted as the water peak). In addition, its low-frequency side seems extending to lower frequencies as the K_2CO_3 molarity increases.

Without any spectrum-smoothing, a simple background correction was performed on these spectra. The CO_3^{2-} peak (~1060 cm^{-1}) was readily fitted with a Gaussian + Lorentz distribution function to derive the peak position, peak height, and peak area.

Fitting the complex water peak is however a troublesome issue. Many attempts have been conducted, but no general agreement has been reached, in terms of the number of band components, the band assignment, and the exact structure of water (e.g., Ratcliffe and Irish, 1982; Walrafen and Chu, 1995; Azbej et al., 2007; Sun, 2009; Sun et al., 2010; Wu and Zheng, 2010). For example, Sun (2009) deconvoluted the water peak into 5 band components whereas Sun and Qin (2011) and Sun et al. (2010) used only two band components to fit it.

We have tried different procedures to fit the water peak, and found that the following method achieves the best internal consistency for our Raman data. Firstly, we set three Gaussian + Lorentz bands at ~3230,

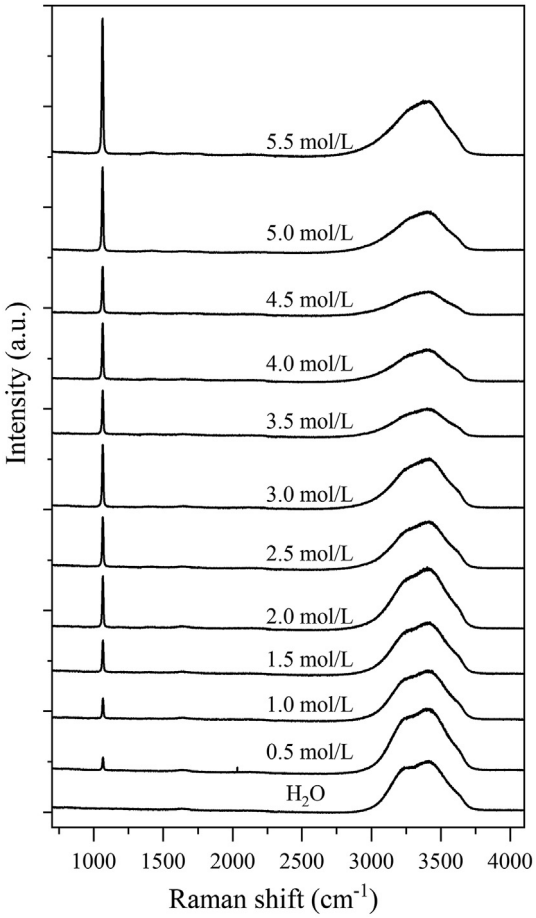

Fig. 3. Raman spectra of water and K_2CO_3 aqueous solutions. Numbers along the spectra refer to the K_2CO_3 molarities.

~3430, and ~3560 cm^{-1}, where the major Raman band components should appear (Sun, 2009; black bands in Fig. 4), and ran the Peakfit v4.12 software many times to fit the water peak as close as possible. Secondly, two weak band components at ~3014 and ~3635 cm^{-1} were manually added, based on the band assignment from Sun (2009; blue bands in Fig. 4), and carefully adjusted to make the sum spectrum matching the original spectrum as close as possible. Thirdly, we ran the Peakfit v4.12 software for three or four times to achieve a better R^2. Usually, this final step only slightly modified all the five band components. This fitting procedure did not mathematically generate a data-fitting result with the minimum R^2, we however tend to believe that it practically reproduces the water peak better, with the fitting result potentially bearing more physical meanings.

3.2.2. Correlations of Raman features and K_2CO_3 concentrations

The relevant Raman features of our studied solutions are listed in Table 1.

As shown in Fig. 5, there is a well-defined monotonic correlation between the peak position of the C–O symmetric stretching mode at ~1060 cm^{-1} and the CO_3^{2-} ion concentration of our studied solutions. This correlation could be used to quantify the solutions. On one hand, our data suggest that as the CO_3^{2-} ion concentration increases from 0 to 5.5 mol/L the peak position changes from ~1066.7 to ~1063.1 cm^{-1}, readily detected by the Raman spectroscopic method. This observation is in general agreement with Sun and Qin (2011) and Rudolph et al. (2006). On the other hand, there are obvious differences among the trends obtained for the K_2CO_3 aqueous solutions using different Raman spectrometers in different laboratories, which unfortunately may hamper the quantification application. Both Sun and Qin (2011) and Rudolph et al. (2006) used the 514.5 nm laser to perform the experiments, but their trends not only located at different energies, but also showed different curvatures (Fig. 5), suggesting interlaboratory difference in the measurements. This study used the 532 nm laser, but obtained a trend at much lower energy (~1.8 cm^{-1}) than Sun and Qin (2011), implying a potential influence of the laser system.

There is a promising point in Fig. 5 though. The Raman spectra recorded for the K_2CO_3 aqueous solutions and the Na_2CO_3 aqueous solutions by using the same experimental setups are well mixed (Rudolph et al., 2006; Sun and Qin, 2011), suggesting that different cations in the carbonate-bearing aqueous solutions might have negligible roles on the energy status of the C–O symmetric stretching vibration. Note that Rudolph et al. (2006) once plotted the concentrations of their K_2CO_3 aqueous solutions and Na_2CO_3 aqueous solutions in mol/kg, and obtained a different conclusion. Since the Raman signal is induced by the activated scattering centers within the excitation volume instead of the excitation mass (Moritz, 1999; Schabel, 2005; Smith and Dent, 2005; Thomas et al., 2009), it is more appropriate to plot the data in mol/L rather than in mol/kg.

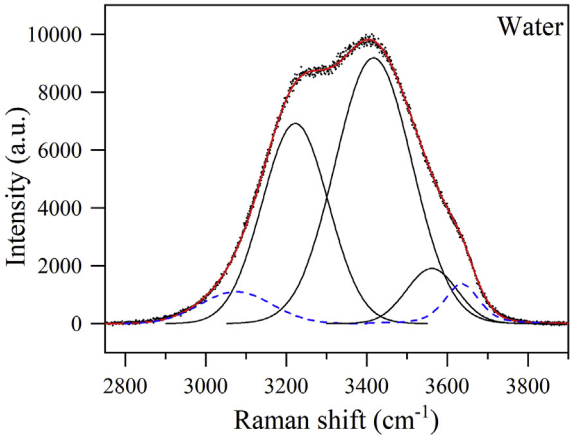

Fig. 4. An example of deconvoluting the water peak (Raman spectrum for pure water). The initial measurement is represented by the black dots, the band components by the solid curves in black and the broken curves in blue, and the sum of the band components by the solid curve in red (see text for more details).

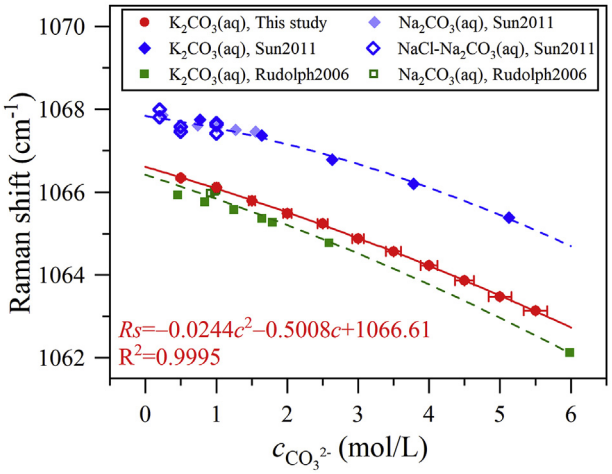

Fig. 5. Raman shift of the CO_3^{2-} peak vs. CO_3^{2-} molarity (mol/L). Rudolph2006, Rudolph et al. (2006); Sun2011, Sun and Qin (2011). K_2CO_3 represents K_2CO_3 aqueous solutions, Na_2CO_3 represents Na_2CO_3 aqueous solutions, and NaCl–Na_2CO_3 represents the NaCl-bearing Na_2CO_3 aqueous solutions. The blue curve was drawn by fitting all data from the K_2CO_3, Na_2CO_3, and NaCl–Na_2CO_3 aqueous solutions from Sun and Qin (2011). The green curve was determined by fitting all data from the K_2CO_3 and Na_2CO_3 aqueous solutions from Rudolph et al. (2006). Sun and Qin (2011) performed their experiments using a Renishaw 1000 Raman spectrometer and a 514.5 nm laser. Rudolph et al. (2006) conducted their experiments using a T 64000 Raman spectrometer and a 514.5 nm laser. Note that the density data of the Na_2CO_3 aqueous solutions at 20 °C from Söhnel and Novotny (1985) were used in the calculation.

The fine structural features of the combination band of the antisymmetric stretching and bending vibrations of the molecular water at ~5180 cm^{-1} show correlations with the salinity of the NaCl, KCl, $CaCl_2$, and $MgCl_2$ aqueous solutions (Kagi et al., 2006), implying potential correlations between some of the Raman features of the water peak and the CO_3^{2-} concentrations of the carbonate-bearing aqueous solutions. Fig. 6 shows the dependence on the CO_3^{2-} concentration of the Raman shift, the fraction of intensity (*F. I.*), and the fraction of area (*F. A.*) of the five band components of the water peak. When the K_2CO_3 molarity increases, the band component at ~3066 cm^{-1} shifts to lower energy (Fig. 6a), the two band components at ~3229 and 3428 cm^{-1} shift to higher energy (Fig. 6b and c), and the rest two band components generally maintain their energy status (Fig. 6d and e). The variations of the *F. I.* and *F. A.* values of the band components with the K_2CO_3 molarity may be used to probe the local hydrogen-bonded networks of the water molecules in the carbonate-bearing aqueous solutions. Sun (2009) proposed that these five band components could be closely related to the local hydrogen-bonded networks of the water molecules, and classified the water molecules into five categories, DAA-OH (~3014 cm^{-1}), DDAA-OH (~3226 cm^{-1}), DA-OH (~3432 cm^{-1}), DDA-OH (~3572 cm^{-1}) and free OH (~3636 cm^{-1}), with D standing for a proton donor and A referring to a proton acceptor. According to his theory, Fig. 6 suggests that as the K_2CO_3 molarity increases, the abundances of both the DAA-OH type (Fig. 6f and k) and the DDAA-OH type (Fig. 6g and l) of water molecules increase whereas those of the rest three types of water molecules decrease (respectively Fig. 6h and m, 6i and n, and 6j and o). Therefore, adding more K_2CO_3 into the carbonate-bearing aqueous solutions promotes the formation of large water molecule clusters, which may significantly alter the physical and chemical properties of the solutions.

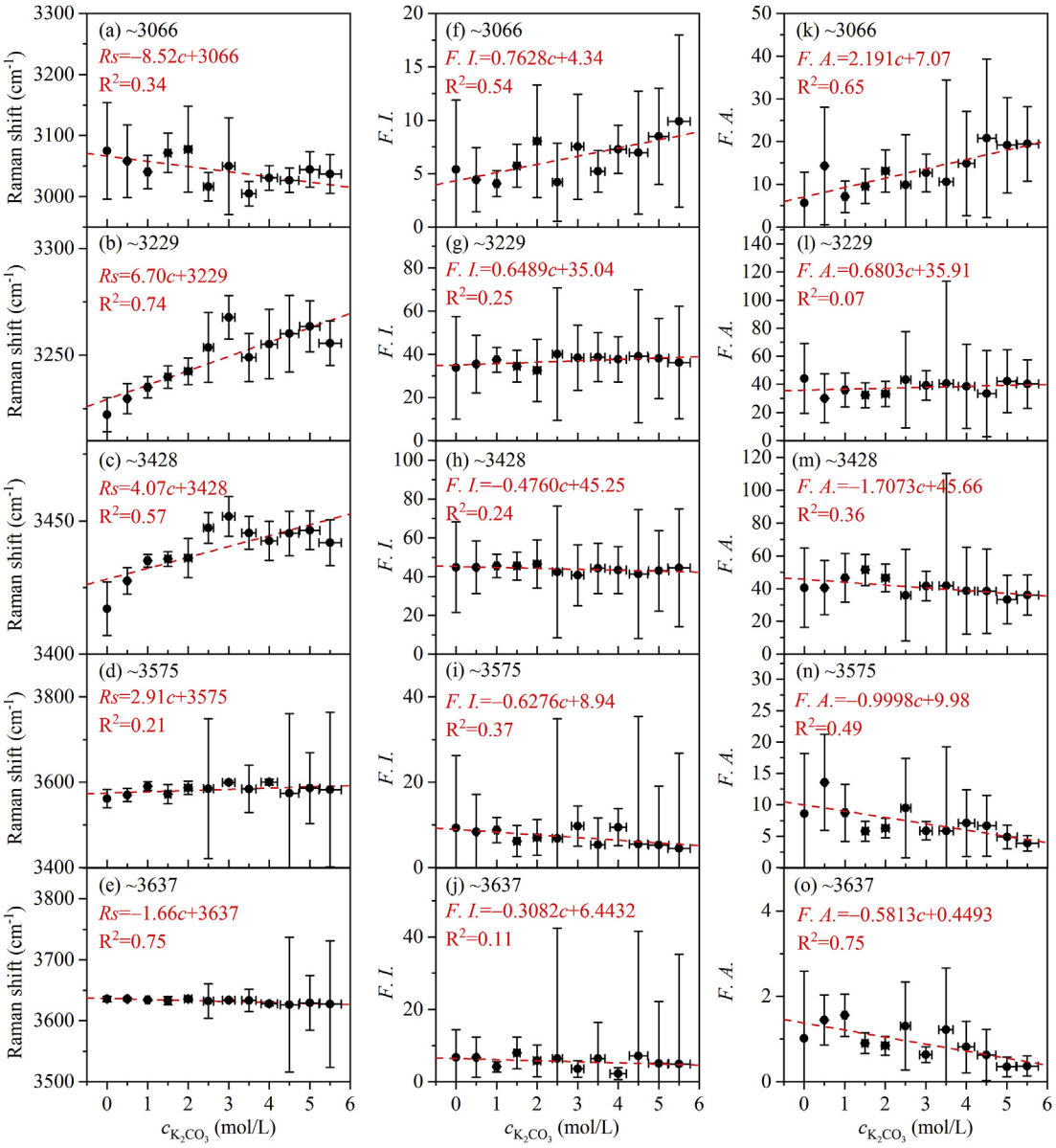

Fig. 6. Dependence on the K_2CO_3 molarity of the peak position (a, b, c, d, e), the fraction of the peak intensity (f, g, h, i, j), and the fraction of the peak area (k, l, m, n, o) of the five band components of the water peak. *F. I.*, fraction of the peak intensity; *F. A.*, fraction of the peak area. The intensity and area of the water peak are derived by summing up the intensity and area of the five band components, respectively.

3.2.3. *Quantify K_2CO_3 concentrations with water as an internal standard*

Using the relative Raman intensity (*R. I.*) of the CO_3^{2-} peak over the water peak should be a much better method to quantify the CO_3^{2-} concentration due to its potentials in eliminating the differences caused by different experimental setups and the instrumental fluctuation of any specific Raman spectrometer (Sun and Qin, 2011). The theoretical foundation is the relationship between the Raman scattering intensity and the concentration of the activated species (Moritz, 1999; Schabel, 2005; Smith and Dent, 2005; Thomas et al., 2009):

$$I = N \times K \times l \times \alpha^2 \times \omega^4 \tag{1}$$

where I stands for the Raman intensity, N is the number of the scattering centers, l is the laser power, ω is the frequency of the incident radiation, α is the polarizability of the electrons in the molecule, and K is a constant which includes many other constants such as the Avogadro constant, the detector efficiency, and so on. The specific value of α and the constants embedded in the K are nearly impossible to be measured so that the absolute Raman intensity is not suitable for direct quantification. But with two Raman active species (denoted as a and b) in a fluid phase, Eq. (1) leads to the following equation, which can be used to determine the relative concentration of the two species ($\frac{c_a}{c_b}$; Lu et al., 2008; Chou and Wang, 2017),

$$\frac{I_a}{I_b} = \frac{N_b}{N_a} \times \frac{K_a}{K_b} \times \frac{\alpha_a^2}{\alpha_b^2} \times \frac{\omega_a^4}{\omega_b^4} = \frac{c_a}{c_b} \times \frac{\eta_a}{\eta_b} \times \frac{\sigma_a}{\sigma_b} = \frac{c_a}{c_b} \times \frac{F_a}{F_b} \tag{2}$$

where η is the instrumental efficiency (nearly equal to K in Eq. (1)), σ is the Raman scattering cross-section ($\sigma = \alpha^2 \times \omega^4$), and F is the Raman quantification factor ($F = \eta \times \sigma$). Clearly the relative Raman intensity ($\frac{I_a}{I_b}$) might be in simple correlation with the relative concentration of the two species ($\frac{c_a}{c_b}$).

As shown in Fig. 7, both our experimental data and the data of Sun and Qin (2011) for the K_2CO_3 aqueous solutions suggest that the relative concentration of the two species CO_3^{2-} and H_2O ($\frac{c_{CO_3^{2-}}}{c_{H_2O}}$) is almost linearly

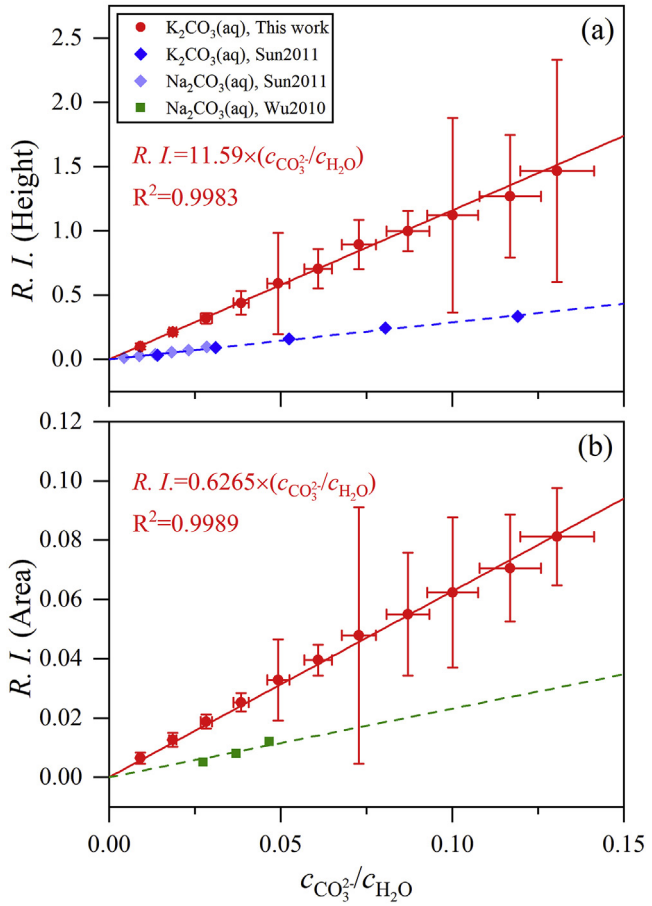

Fig. 7. Relative Raman intensity (*R. I.*) of the CO_3^{2-} peak over the water peak versus relative molarity of the CO_3^{2-} ion over the H_2O: (a) scattering intensity; (b) scattering area. The intensity and area of the water peak are determined by summing up the intensity and area of the five band components, respectively. Sun2011, Sun and Qin (2011); Wu2010, Wu and Zheng (2010). K_2CO_3 represents K_2CO_3 aqueous solutions, and Na_2CO_3 represents Na_2CO_3 aqueous solutions. The experimental setups and analytical conditions in Sun and Qin (2011) and in Wu and Zheng (2010) were generally identical, with a Renishaw 1000 Raman Spectrometer (Gloucestershire, UK), a Ar^+ laser with 514.5 nm, a 50 μm entrance slit, and 1 scan. The differences were the laser power and data-collecting time, being 25 mW and 30 s in Sun and Qin (2011) but 20 mW and 10 s in Wu and Zheng (2010). Note that the density data of the Na_2CO_3 aqueous solutions at 20 °C from Söhnel and Novotny (1985) were used in the calculation.

correlated with the relative Raman intensity ($\frac{I_{CO_3^{2-}}}{I_{H_2O}}$). Since all data points from either study fall on a straight line, the Raman quantification factors ratio ($\frac{F_{CO_3^{2-}}}{F_{H_2O}}$) in one study then must be a constant. This means that either the Raman quantification factors $F_{CO_3^{2-}}$ and F_{H_2O} are independent to the composition of the K_2CO_3 aqueous solutions, or their compositional dependences are coupled in a special way so that these dependences cancel each other out. Consequently, the Raman O–H stretching band of water can be used as an internal standard to determine the carbonate concentrations of the carbonate-bearing aqueous solutions.

Nevertheless, the data from this study and from Sun and Qin (2011) fall on straight lines with different slopes (Fig. 7), indicating the importance to carry out some calibration experiments to constrain the Raman quantification factors ratio ($\frac{F_{CO_3^{2-}}}{F_{H_2O}}$) for a specific Raman spectrometer and its analytical conditions. It is well known that when single Raman band is used in the quantification, extensive and cumbersome calibration experiments are required in order to establish a specific correlation curve

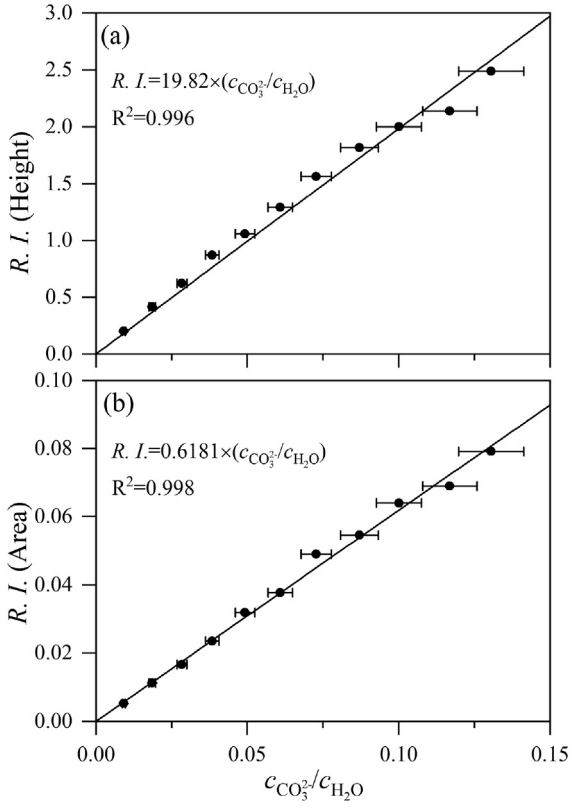

Fig. 8. Relative Raman intensity (*R. I.*) of the CO_3^{2-} peak over the water peak versus relative molarity of the CO_3^{2-} ion over the H_2O: (a) scattering intensity; (b) scattering area. Raman intensity data are directly measured from our spectra without deconvoluting.

for a specific Raman spectrometer with specified data-collecting conditions. The calibration process however can be very simple when the Raman quantification factors ratio is employed in the quantification. The linear correlations shown in Fig. 7 suggest that the Raman quantification factors ratio ($\frac{F_{CO_3^{2-}}}{F_{H_2O}}$) can be easily established by performing just one high-quality experiment, and then can be used to quantify other unknown K_2CO_3 aqueous solutions, provided that the same experimental protocol is followed.

Since the experimental data for the K_2CO_3 aqueous solutions and the Na_2CO_3 aqueous solutions collected using the same Raman spectrometer with the same analytical conditions (Sun and Qin, 2011) fall on the same straight line, further, Fig. 7 implies that the Raman quantification factors ratio ($\frac{F_{CO_3^{2-}}}{F_{H_2O}}$) for these two composition systems are essentially identical. Hence, the calibration established for the K_2CO_3 or Na_2CO_3 aqueous solutions may be directly used to quantify the Na_2CO_3 or K_2CO_3 aqueous solutions. It is presently unclear whether or not this phenomenon extends to other carbonate-bearing aqueous solutions.

To further simplify the quantifying process, we may pay no much attention to the specific fine spectroscopic features of the CO_3^{2-} peak and the water peak, but use their entire scattering intensities or areas directly extracted from the Raman spectra. This has been demonstrated in Fig. 8, with the data listed in Table 2.

3.3. *IR features of K_2CO_3 aqueous solutions and quantification*

This study aimed at the *P* condition of 1 atm, and all the IR spectra reported for our studied solutions were collected from the rim positions of the pseudo-Newton's rings (Fig. 1), where the pressure was expected to be equal to the room *P*. To illustrate this point further, a series of IR spectra for the ion-distilled water sample were collected along a profile

Table 2
Raman scattering intensities of water and K_2CO_3 aqueous solutions directly measured from the Raman spectra.

		CO_3^{2-}		H_2O		CO_3^{2-}/H_2O	
c (mol/L)	c (CO_3^{2-})/c (H_2O)[a]	I_{Height}	I_{Area} (cm^{-1})	I_{Height}	I_{Area} (cm^{-1})	*R. I.* (Height)	*R. I.* (Area)
0.00 (0)[b]	0.000 (0)			9988	4,305,620		
0.50 (2)	0.009 (1)	2458	28,648	12,317	5,396,990	0.20	0.01
1.00 (3)	0.019 (1)	3934	48,243	9464	4,279,416	0.42	0.01
1.50 (5)	0.028 (2)	6294	73,107	10,141	4,396,376	0.62	0.02
2.00 (6)	0.038 (3)	10,092	123,735	11,624	5,265,940	0.87	0.02
2.50 (8)	0.049 (4)	9785	129,988	9280	4,081,311	1.05	0.03
3.00 (9)	0.061 (5)	12,339	160,994	9570	4,270,404	1.29	0.04
3.50 (11)	0.073 (6)	8562	117,285	5480	2,391,649	1.56	0.05
4.00 (12)	0.087 (7)	11,160	150,606	6144	2,761,501	1.82	0.05
4.50 (14)	0.100 (8)	9236	125,869	4615	1,968,210	2.00	0.06
5.00 (15)	0.117 (10)	16,580	234,654	7752	3,403,077	2.14	0.07
5.50 (17)	0.131 (12)	26,696	375,411	10,730	4,745,671	2.49	0.08

[a] This refers to the relative concentration of the CO_3^{2-} ion (mol/L) to the H_2O (mol/L) calculated according to the measured density.
[b] Number in parentheses is one standard deviation in the rightmost digit. The concentration errors of the K_2CO_3 aqueous solutions are assumed as 3%.

from the rim position towards the center position of the pseudo-Newton's rings (Fig. 1). The spectra are shown in Fig. 9. Clearly, there is no detectable position dependence of the water peak (all at ~3417 cm^{-1}), suggesting no *P* gradient at least for the investigated portion of the pseudo-Newton's rings (Sun et al., 2003; Kawamoto et al., 2004).

3.3.1. IR features of K_2CO_3 aqueous solutions

Fig. 10 shows the transmission IR spectra of our ion-distilled water and K_2CO_3 aqueous solutions. The doublet peak at ~2350 cm^{-1} stands for the antisymmetric stretching mode of gaseous CO_2, and is irrelevant. The IR peak at ~1400 cm^{-1} represents the C–O antisymmetric stretching vibration of the CO_3^{2-} ion. It does not change its peak position, but becomes stronger as the K_2CO_3 molarity increases. Due to potential peak splitting caused by strong hydration (Rudolph et al., 2008), it gradually becomes more asymmetric. This asymmetry is especially prominent in the spectra taken from the 4.5, 5.0, and 5.5 mol/L K_2CO_3 aqueous solutions (Fig. 10).

There are mainly two IR peaks for the solvent water. The IR peak at ~1655 cm^{-1} represents the O–H bending vibration, and shows no obvious changes in both the peak position and the peak shape as the K_2CO_3 molarity of our aqueous solutions varies. The broad IR peak centering at ~3417 cm^{-1} stands for the O–H stretching vibration. Its peak position slowly and gradually shifts to lower energy as the K_2CO_3 molarity of our studied solutions increases. Additionally, its low-frequency side extends to lower wavenumbers, presumably suggesting stronger hydrogen-bonding at high K_2CO_3 concentrations. Former studies have proposed that this broad water peak can be decomposed into three Gaussian components at ~3603, 3465, and 3300 cm^{-1}, and assigned them respectively to free water molecules (~3603 cm^{-1}), water molecules with one hydrogen bond (~3465 cm^{-1}), and water molecules with two hydrogen bonds (~3300 cm^{-1}; e.g., Buijs and Choppin, 1963; MacDonald et al., 1986; Jain et al., 1989; Freda et al., 2005). Well in line with our Raman observation, these IR data hence suggest that as the K_2CO_3 concentration increases, the water molecules in the aqueous solution are more hydrogen-bonded and form more large clusters.

3.3.2. Removing interference fringes and fitting IR spectra

The baselines of our IR spectra in a relatively narrow energy range from ~1000 to 4500 cm^{-1} appear generally regular and thus cause no tremendous problem in determining the absorbance of the peaks (Fig. 10). In a wider energy range, however, interference fringes can be clearly observed (Fig. 11; from ~1000 to 7000 cm^{-1}), and their influence should be removed before the quantification is executed. For eliminating

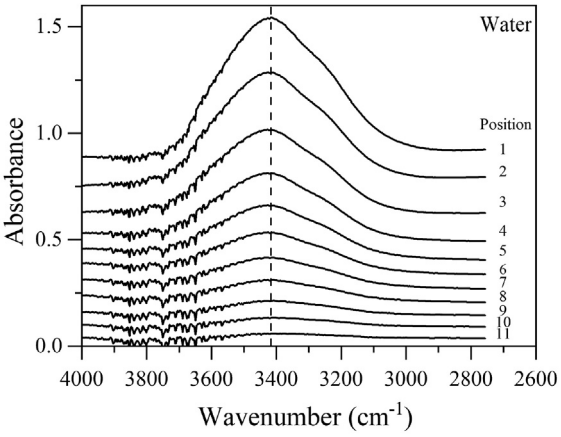

Fig. 9. Water infrared spectra collected along the profile from the rim position (Position 1) towards the center position (Position 11) of the pseudo-Newton's rings, as shown in Fig. 1. According to Weng et al. (1985), the thickness of our wedged thin film decreased from ~1.422 μm (absorbance height = ~0.641) at Position 1 to ~0.065 μm (absorbance height = ~0.020) at Position 11.

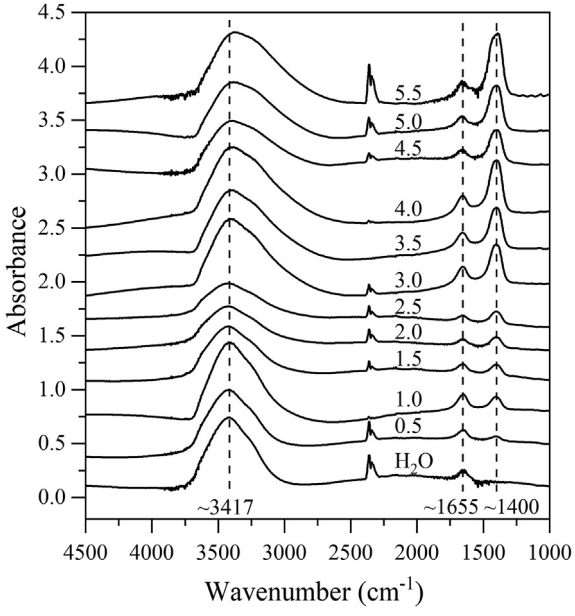

Fig. 10. Infrared spectra of our water and K_2CO_3 aqueous solutions. Numbers along the spectra refer to the K_2CO_3 molarities. Note that the peak representing the O–H bending vibration at ~1655 cm^{-1} starts to overlap with the peak of the C–O stretching vibration band at ~1400 cm^{-1} at some K_2CO_3 molarity between 2.5 and 3 mol/L. This peak-overlapping at high K_2CO_3 molarities leads to relatively large uncertainty in measuring the absorbances of these two peaks.

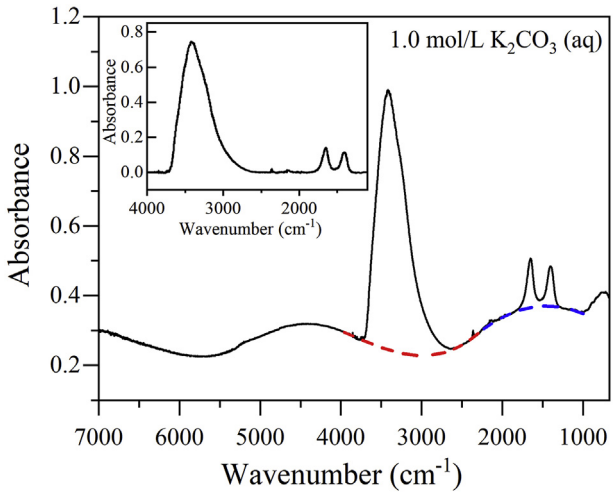

Fig. 11. Interference fringe-removing by eye-fitting the spectrum baseline (example spectrum for the 1.0 mol/L K_2CO_3 aqueous solution). Red and blue dashed curves represent the baselines for the two corresponding sections of the original spectra (black curve; drawn with the Peakfit v4.12 software). The insert shows the interference fringe-removed spectrum.

the interference fringes from IR spectra, different methods have been developed (e.g., Martens and Stark, 1991; Bréhat and Wyncke, 1992; 1997; Maley, 1992; Jena and Hore, 2011; Dekkers et al., 2013; Konevskikh et al., 2015; Azarfar et al., 2018). Rather unfortunately, our IR spectra show 1–2 complete interference periods only so that none of the existing techniques can be successfully applied to them. Eventually we have decided to eye-fit the spectrum baselines, as illustrated in Fig. 11.

This eye-fitting procedure has been verified by the IR spectra of the ion-distilled water, which were collected along the profile shown in Fig. 1e. For simplicity, we only show the results for the first four IR analyses. The positions of the IR analyses at Positions 1 to Position 4 were next to each other, with a distance of 50 μm (note the 50-μm diameter of the IR beam). Since the thickness of the wedged thin film was <2 μm (See the caption of Fig. 9), it should be reasonable to assume that the equal distance of the four adjacent IR analyses has caused the averaged thickness of the films at these positions evenly decreasing from Position 1 to Position 4. As dictated by the Beer-Lambert Law, the peak absorbances then should be in linear correlations with the positions, provided that the eye-fitting baseline correction and the band-component deconvolution of the spectrum led to no other complications. By following the deconvoluting scheme for the IR spectra of pure water outlined in the literature (Freda et al., 2005; more discussion later), and adopting the above eye-fitting baseline correction procedure, we have indeed obtained linear correlations between the IR features and the positions of the IR analyses (Fig. 12). It follows that our eye-fitting baseline correction procedure to remove the weak interference fringes must have been successful in general.

Deconvoluting the water peak in the IR spectrum of the pure water (Fig. 13a) was easily accomplished by running the Peakfit v4.12 software. Based on the results of Freda et al. (2005; references therein), three Gaussian + Lorentz bands at ~3300, ~3465, and ~3603 cm^{-1} were used as the inputs in the deconvolution. As shown in Fig. 13a, the final peak positions of the component bands are essentially identical to the inputs, suggesting that this deconvolution procedure has been very successful in the cases of the ion-distilled water.

However, this deconvolution procedure could not be well applied to the IR spectra taken from the K_2CO_3 aqueous solutions, as shown by the example in Fig. 13b. Different deconvolution procedures were tested with significantly different results obtained (see Fig. 13c for one example). A similar phenomenon, with no unique solution from the

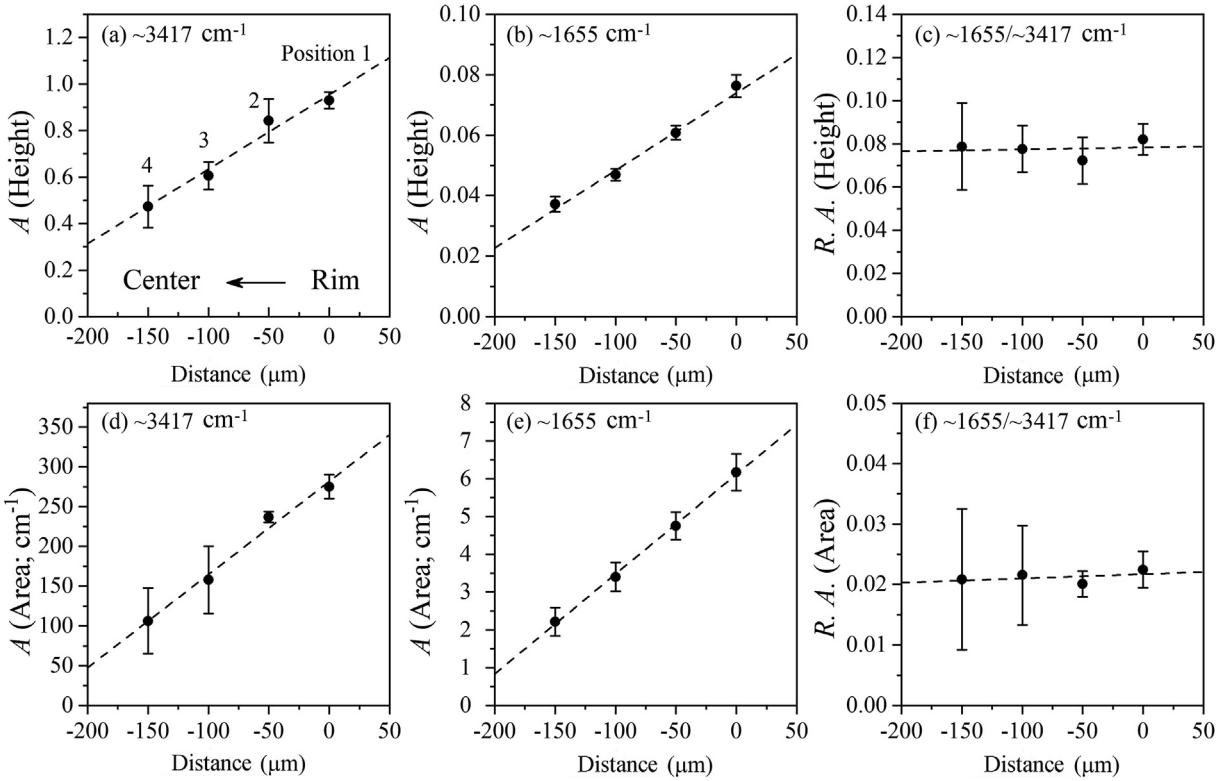

Fig. 12. Correlations observed for the ion-distilled water between the analyzed position and the IR absorbance (*A*) of the O–H stretching vibration peak at ~3417 cm^{-1} and/or bending vibration peak at ~1655 cm^{-1}: (a) Absorbance height of peak at ~3417 cm^{-1}; (b) Absorbance height of peak at ~1655 cm^{-1}; (c) Relative absorbance (*R. A.*) height of peaks at ~3417 and ~1655 cm^{-1}; (d) Absorbance area of peak at ~3417 cm^{-1}; (e) Absorbance area of peak at ~1655 cm^{-1}; (f) Relative absorbance (*R. A.*) area of peaks at ~3417 and ~1655 cm^{-1}.

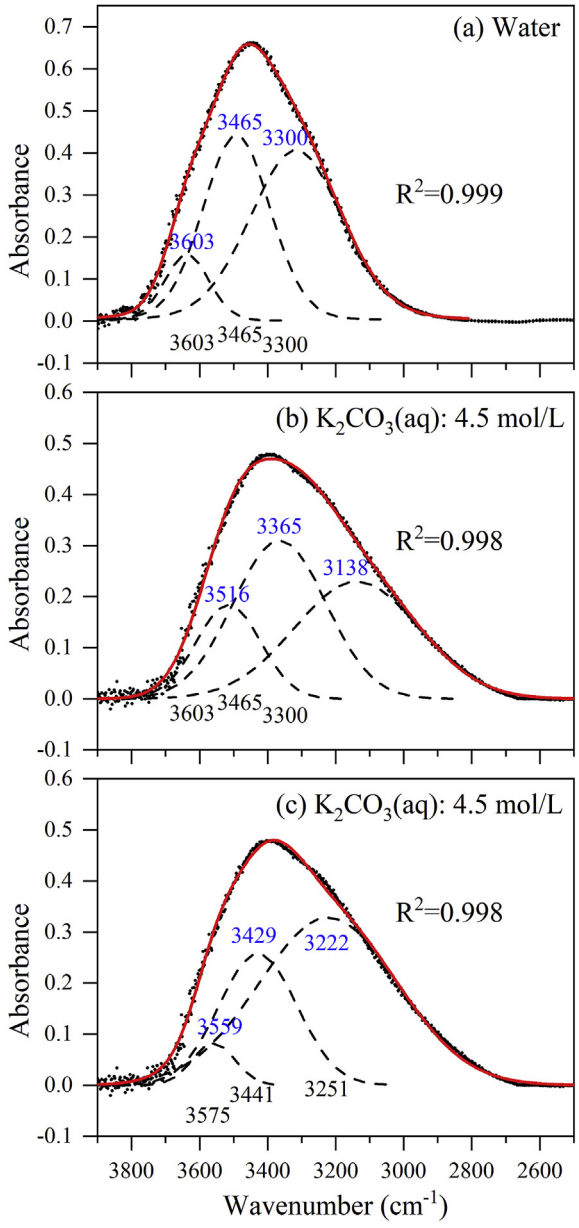

Fig. 13. Representative band component analyses for the broad and generally feature-less water peak at ~3417 cm^{-1}: (a) pure water; (b) and (c) 4.5 mol/L K_2CO_3 aqueous solution. The numbers in black in (a), (b), and (c) are the initial inputs whereas the numbers in blue are the final peak positions for the band components derived by running the Peakfit v4.12 software. The deconvoluting process in both (a) and (b) was started with adding three peak components from Freda et al. (2005), whereas the deconvoluting process in (c) was started with an arbitrary and manual introduction of three band components which reproduced the experimental spectrum as close as possible.

deconvoluting process, was observed by Kagi et al. (2006) while they carried out their band component analyses on the antisymmetric stretching + bending combination IR band (~5180 cm^{-1}) of some salt aqueous solutions. Since the broad water peak at its low frequency side has a more and more prominent tail extending to lower and lower wavenumbers as the K_2CO_3 concentration of the K_2CO_3 aqueous solutions increases (Fig. 10), more band components with various peak positions and peak heights may be required to reproduce it. No doubt that our understanding of the IR features of the aqueous solutions is presently in its infant phase. We have hence decided to measure the peak absorbance directly from the spectra without any deconvoluting. The results are listed in Table 3.

3.3.3. *Quantify K_2CO_3 concentrations with IR data*

Even with thin fluid films, the C–O antisymmetric stretching vibration of the CO_3^{2-} ion, and the O–H stretching and bending vibrations of water all produce strong IR signals (Fig. 10). It follows that a relative IR absorbance method (*R. A.*) can be effectively established.

We start with the Beer-Lambert Law. It states that the absorbance of one certain peak (*A*; dimensionless) is the common logarithm of the ratio of the transmitted IR intensity (*I*) over the incident IR intensity (I_0), and is proportional to the molar concentration (*c*; mol/L), the molar absorptivity of this peak (ε; L/(mol·cm)), and the distance of the light path (*l* in cm; equal to the sample thickness *d* in cm). Its general form is as following,

$$A = -\log_{10}\frac{I}{I_0} = \varepsilon \times l \times c. \tag{3}$$

In Earth sciences, the Beer-Lambert Law transforms into the next equation,

$$w = \frac{M \times A}{d \times \rho \times \varepsilon} \times 100 \tag{4}$$

where *w* stands for the concentration in wt.%, *M* refers to the molar mass in g/mol, ρ is the density in g/L. Clearly, its application requires that all the parameters *d*, ρ, and ε are known for the sample under investigation. For micro fluid inclusions, unfortunately, accurate measurements of their thickness and density can be extremely difficult, if not entirely impossible. Further, the molar absorptivity (ε) for certain vibration mode is not always available and may significantly change with the composition of the fluids.

These difficulties can be successfully avoided by employing the relative IR absorbance method. The relative IR absorbance ($\frac{A_a}{A_b}$) can be related to the relative concentration ($\frac{c_a}{c_b}$) of two species a and b, as following,

$$\frac{A_a}{A_b} = \frac{M_b}{M_a} \times \frac{w_a}{w_b} \times \frac{\varepsilon_a}{\varepsilon_b} = \frac{c_a}{c_b} \times \frac{\varepsilon_a}{\varepsilon_b} \tag{5}$$

with the parameters d_a and d_b, ρ_a and ρ_b cancelled for the same measurement. If both ε_a and ε_b are not respectively dependent on the concentrations of the species a and b, or if these dependences coincidently lead to a constant $\frac{\varepsilon_a}{\varepsilon_b}$, the relative IR absorbance ($\frac{A_a}{A_b}$) then should be in a linear correlation with the relative concentration of the two species ($\frac{c_a}{c_b}$).

The results of our experiments are shown in Figs. 14 and 15.

For the two major water peaks at ~1655 and 3417 cm^{-1}, their relative IR absorbance is only weakly dependent on the relative concentration of the two species CO_3^{2-} and H_2O ($\frac{c_{CO_3^{2-}}}{c_{H_2O}}$) in the K_2CO_3 aqueous solutions (Fig. 14). The correlation between them should therefore have little use in quantifying the concentration of the CO_3^{2-} ion.

In comparison, the relative absorbance of the IR peak of the C–O antisymmetric stretching vibration of the CO_3^{2-} ion at ~1400 cm^{-1} and that of the O–H stretching vibration at ~3417 cm^{-1} has much stronger dependence on the relative concentration of the two species CO_3^{2-} and H_2O ($\frac{c_{CO_3^{2-}}}{c_{H_2O}}$) in the K_2CO_3 aqueous solutions (Fig. 15). For the data at $c_{K_2CO_3} < \sim 3$ mol/L, further, the correlation is essentially linear in all cases, suggesting that the molar absorptivities ratio ($\frac{\varepsilon_{CO_3^{2-}}}{\varepsilon_{H_2O}}$) is a constant. It follows that the relative absorbance of these two IR peaks can be calibrated as a means to characterize the CO_3^{2-} concentration in the K_2CO_3 aqueous solutions. Taking into account the results derived from the Raman data, this conclusion may be extended to the case of the Na_2CO_3 aqueous solutions.

The deviation of the experimental data at $c_{K_2CO_3} > \sim 2.5$ mol/L from the linear correlation established by the experimental data at $c_{K_2CO_3} < \sim 3$ mol/L is mostly caused by the overlapping of the O–H bending vibration band at ~1655 cm^{-1} and the C–O antisymmetric stretching

Table 3
IR features of water and K_2CO_3 aqueous solutions.

		Peak height[a]			*R.A.*(Height)			Peak area (cm^{-1})[a]			*R.A.*(Area)		
***c*(mol/L)**	***c*(CO_3^{2-})/*c*(H_2O)[b]**	***A*$_{\sim1400}$**	***A*$_{\sim1655}$**	***A*$_{\sim3417}$**	**1655/3417[c]**	**1400/1655**	**1400/3417**	***A*$_{\sim1400}$**	***A*$_{\sim1655}$**	***A*$_{\sim3417}$**	**1655/3417**	**1400/1655**	**1400/3417**
0.00 (0)[d]	0.000 (0)		0.088	0.662	0.132				6.144	268.87	0.023		
0.50 (2)	0.009 (1)	0.035	0.078	0.591	0.132	0.449	0.059	3.071	8.238	252.98	0.033	0.373	0.012
1.00 (3)	0.019 (1)	0.116	0.144	0.739	0.195	0.806	0.157	12.646	15.401	323.46	0.048	0.821	0.039
1.50 (5)	0.028 (2)	0.090	0.071	0.486	0.146	1.268	0.185	9.115	7.058	232.69	0.030	1.291	0.039
2.00 (6)	0.038 (3)	0.097	0.058	0.352	0.165	1.672	0.276	9.881	5.627	169.57	0.033	1.756	0.058
2.50 (8)	0.049 (4)	0.109	0.050	0.320	0.156	2.180	0.341	11.936	5.195	161.52	0.032	2.298	0.074
3.00 (9)	0.061 (5)	0.364	0.185	0.648	0.285	1.968	0.562	46.221	24.955	328.79	0.076	1.852	0.141
3.50 (11)	0.073 (6)	0.378	0.158	0.595	0.266	2.392	0.635	46.697	18.716	306.65	0.061	2.495	0.152
4.00 (12)	0.087 (7)	0.506	0.205	0.631	0.325	2.468	0.802	67.470	27.957	340.62	0.082	2.413	0.198
4.50 (14)	0.100 (8)	0.289	0.083	0.493	0.168	3.482	0.586	34.042	7.466	275.08	0.027	4.560	0.124
5.00 (15)	0.117 (10)	0.405	0.122	0.541	0.226	3.320	0.749	52.534	16.446	291.97	0.056	3.194	0.180
5.50 (17)	0.131 (12)	0.580	0.164	0.607	0.270	3.537	0.956	78.833	27.699	338.02	0.082	2.846	0.233

[a] The peak heights and areas are directly extracted from the IR spectra.
[b] This refers to the relative concentration of the CO_3^{2-} ion (mol/L) to the H_2O (mol/L) calculated according to the measured density.
[c] 1655/3417 means that the relative absorbance is for the IR peak at ~1655 cm^{-1} over the IR peak at ~3417 cm^{-1}.
[d] Number in parentheses is one standard deviation in the rightmost digit. The concentration errors of K_2CO_3 aqueous solutions are assumed as 3%.

vibration band at ~1400 cm^{-1} at these high K_2CO_3 molarities. Whether or not this is correct is unimportant though. When $c_{K_2CO_3}$ = 2.5 mol/L, the concentration of the K_2CO_3 is already 27 wt.% (Supplementary Materials Table S1), presumably much higher than the K_2CO_3 concentrations in most carbonate-bearing aqueous fluids.

4. Conclusions

Carbonate-bearing aqueous fluids are significant geological fluids with wide occurrences, and a method to accurately quantify the carbonate concentration is of high value. By performing Raman and IR spectroscopic measurements on some standard K_2CO_3 aqueous solutions at ambient *P* and *T*, the correlations between some spectroscopic features and the CO_3^{2-} molarity have been revealed in this study. Eventually, some Raman and IR spectroscopic methods with water as internal standards have been established for the quantification of the carbonate concentrations in the carbonate-bearing aqueous fluids.

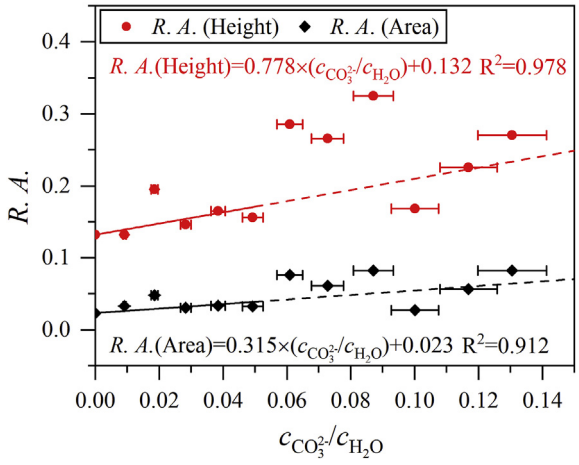

Fig. 14. Relative IR absorbance (*R. A.*) of peak at ~1655 cm^{-1} over peak at ~3417 cm^{-1} versus relative molarity of the CO_3^{2-} ion over the H_2O. Red circles are for the *R. A.* heights whereas black diamonds are for the *R. A.* areas. The equations and the solid lines are for the results obtained from the aqueous solutions with $c_{K_2CO_3}$ < ~3.0 mol/L. The dashed lines represent the extensions of the solid lines to higher $c_{K_2CO_3}$. Due to the overlapping of the O–H bending vibration band (~1655 cm^{-1}) with the C–O stretching vibration band (~1400 cm^{-1}) at $c_{K_2CO_3}$ > ~2.5 mol/L (Fig. 10), there are relatively large uncertainties in the experimental results at high $c_{K_2CO_3}$, which are therefore left out in the regressions. Absorbance data are directly measured from the spectra without any deconvoluting.

Our Raman spectroscopic analyses suggest that the relative Raman intensity ($\frac{I_{CO_3^{2-}}}{I_{H_2O}}$) of the C–O symmetric stretching mode of the CO_3^{2-} ion (at ~1060 cm^{-1}) over the O–H stretching mode of the solvent water (at ~3000–3700 cm^{-1}) is in an almost linear correlation with the relative molarity ($\frac{c_{CO_3^{2-}}}{c_{H_2O}}$) of these two species in the K_2CO_3 aqueous solutions. The correlation between these two variables, or the quantification factors ratio ($\frac{F_{CO_3^{2-}}}{F_{H_2O}}$) of the two species CO_3^{2-} ion and water, can therefore be readily established by performing just one high-quality Raman spectroscopic measurement on one standard K_2CO_3 aqueous solution. On the basis of this calibration, the relative Raman intensity ($\frac{I_{CO_3^{2-}}}{I_{H_2O}}$) of these two Raman peaks in a Raman spectrum can be employed to characterize the concentration of the CO_3^{2-} ion in unknown aqueous solutions if the same Raman spectrometer is used and the same analytical conditions are maintained. By performing experiments on certain standard K_2CO_3 aqueous solution, furthermore, the interlaboratory differences in the Raman spectroscopic measurements can be easily detected.

In comparison, our IR spectroscopic analyses suggest that the relative IR absorbance ($\frac{A_{CO_3^{2-}}}{A_{H_2O}}$) of the C–O antisymmetric stretching vibration mode of the CO_3^{2-} ion (at ~1400 cm^{-1}) over the O–H stretching vibration mode (at ~3417 cm^{-1}) essentially linearly correlates with the relative molarity ($\frac{c_{CO_3^{2-}}}{c_{H_2O}}$) of these two species in the K_2CO_3 aqueous solutions. The correlation between these two variables, or the molar absorptivities ratio ($\frac{\varepsilon_{CO_3^{2-}}}{\varepsilon_{H_2O}}$) of the two species CO_3^{2-} ion and water, can therefore be readily established by performing just one high-quality IR spectroscopic measurement on one standard K_2CO_3 aqueous solution (favorably at $c_{K_2CO_3}$ < 3.0 mol/L). With this calibration or just taking the value of the $\frac{\varepsilon_{CO_3^{2-}}}{\varepsilon_{H_2O}}$ determined in this study (7.030 (220) for the *R. A.* height and 1.525 (82) for the *R. A.* area; Fig. 15), the relative IR absorbance ($\frac{A_{CO_3^{2-}}}{A_{H_2O}}$) of these two IR peaks in an IR spectrum can be employed to characterize the

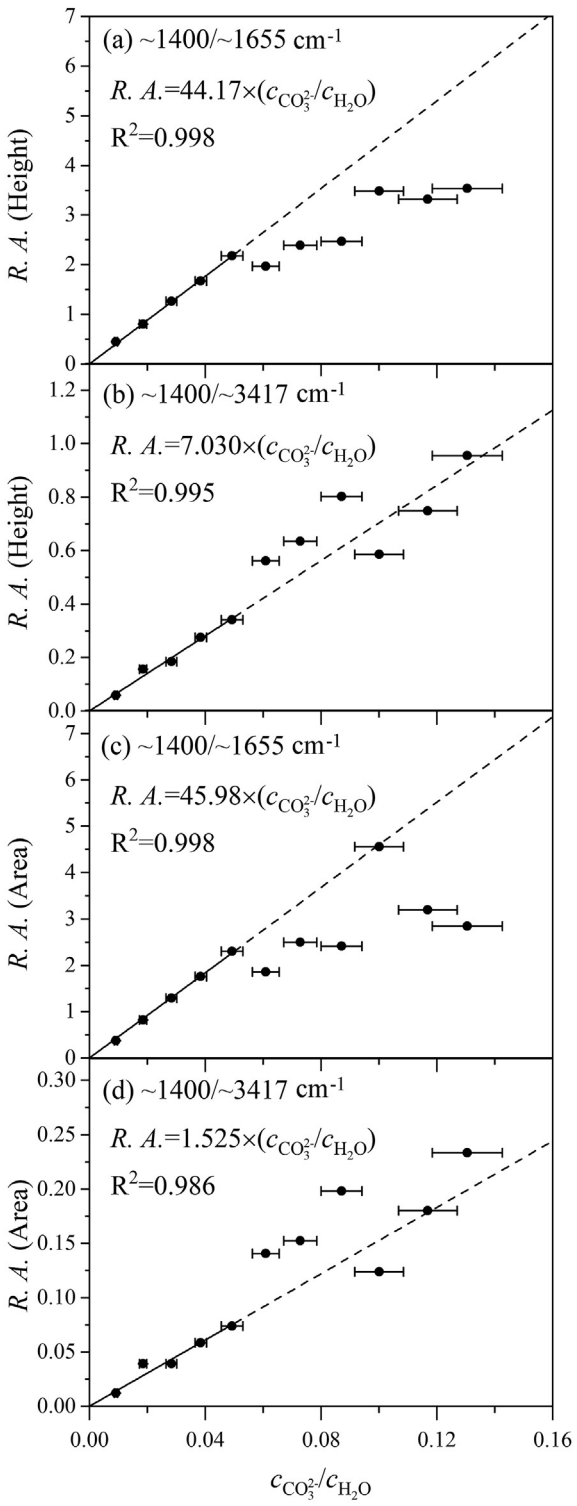

Fig. 15. Relative IR absorbance (*R. A.*) of peak at ~1400 cm^{-1} over peak at ~1655 or at ~3417 cm^{-1} versus relative molarity of the CO_3^{2-} ion over the H_2O. The equations and the solid lines are for the results obtained from the aqueous solutions with $c_{K_2CO_3}$ < ~3.0 mol/L. The dashed lines represent the extensions of the solid lines to higher $c_{K_2CO_3}$. Due to the overlapping of the O–H bending vibration band (~1655 cm^{-1}) with the C–O stretching vibration band (~1400 cm^{-1}) at $c_{K_2CO_3}$ > ~2.5 mol/L (Fig. 10), there are relatively large uncertainties in the experimental results at high $c_{K_2CO_3}$, which are therefore left out in the regressions. Absorbance data are directly measured from the spectra without any deconvoluting.

concentration of the CO_3^{2-} ion in unknown K_2CO_3 aqueous solutions. As the IR signals of these two vibration modes are very strong, this method can be particularly useful in the studies of micro fluid inclusions.

Moreover, the above spectroscopic methods with the O–H stretching vibration mode as the internal standard, when established with the K_2CO_3 aqueous solutions, may be extended to investigate the Na_2CO_3 aqueous solutions, and vice versa.

Declaration of competing interest

The authors declare that they have no known competing financial interests or personal relationships that could have appeared to influence the work reported in this paper.

Acknowledgements

We thank Professor I.-M. Chou for his insightful suggestions to this study. This study was financially supported by the DREAM project of MOST, China (Grant No. 2016YFC0600408), by the Strategic Priority Research Program (B) of Chinese Academy of Sciences (Grant No. XDB18000000), and by the Program of the National Mineral Rock and Fossil Specimens Resource Center from MOST, China.

Appendix A. Supplementary data

Supplementary data to this article can be found online at https://doi.org/10.1016/j.gsf.2020.03.002.

References

Aulbach, S., Stachel, T., Heaman, L.M., Carlson, J.A., 2011. Microxenoliths from the Slave craton: archives of diamond formation along fluid conduits. Lithos 126, 419–434. https://doi.org/10.1016/j.lithos.2011.07.012.

Azarfar, G., Aboualizadeh, E., Walter, N.M., Ratti, S., Olivieri, C., Norici, A., Nasse, M., Kohler, A., Giordano, M., Hirschmugl, C.J., 2018. Estimating and correcting interference fringes in infrared spectra in infrared hyperspectral imaging. Analyst 143, 4674–4683. https://doi.org/10.1039/c8an00093j.

Azbej, T., Severs, M.J., Rusk, B.G., Bodnar, R.J., 2007. In situ quantitative analysis of individual H_2O-CO_2 fluid inclusions by laser Raman spectroscopy. Chem. Geol. 237, 255–263. https://doi.org/10.1016/j.chemgeo.2006.06.025.

Bakker, R.J., Mamtani, M.A., 2000. Fluid inclusions as metamorphic process indicators in the southern aravalli mountain belt (India). Contrib. Mineral. Petrol. 139, 163–179. https://doi.org/10.1007/PL00007669.

Bréhat, F., Wyncke, B., 1992. Theoretical considerations on the reflectivity of anisotropic absorbing crystal plates, measured by infrared spectroscopy. Infrared Phys. 33 (6), 563–573. https://doi.org/10.1016/0020-0891(92)90073-3.

Bréhat, F., Wyncke, B., 1997. Measurement of the optical constants of crystal quartz at 10 K and 300 K in the far infrared spectral range: 10-600 cm^{-1}. Int. J. Infrared Millimet. Waves 18 (9), 1663–1679. https://doi.org/10.1007/bf02678278.

Bühn, B., Rankin, A.H., Schneider, J., Dulski, P., 2002. The nature of orthomagmatic, carbonatitic fluids precipitating REE, Sr-Rich fluorite: fluid-inclusions evidence from the Okorusu fluorite deposit, Namibia. Chem. Geol. 186, 75–98. https://doi.org/10.1016/S0009-2541(01)00421-1.

Buijs, K., Choppin, G.R., 1963. Near-infrared studies of the structure of water. I. Pure water. J. Chem. Phys. 39, 2035–2041. https://doi.org/10.1063/1.1734579.

Chou, I.-M., Wang, A., 2017. Application of laser Raman micro-analyses to Earth and planetary materials. J. Asian Earth Sci. 145, 309–333. https://doi.org/10.1016/j.jseaes.2017.06.032.

Deines, P., 1980. The carbon isotopic composition of diamonds: relationship to diamond shape, color, occurrence and vapor composition. Geochem. Cosmochim. Acta 44, 943–961. https://doi.org/10.1016/0016-7037(80)90284-7.

Dekkers, H.F.W., Gallo, A., van Elshocht, S., 2013. Infrared molar absorption coefficient of H_2O stretching modes in SiO_2. Thin Solid Films 542, 8–13. https://doi.org/10.1016/j.tsf.2013.05.151.

Freda, M., Piluso, A., Santucci, A., Sassi, P., 2005. Transmittance Fourier transform infrared spectra of liquid water in the whole mid-infrared region: temperature dependence and structural analysis. Appl. Spectrosc. 59 (9), 1155–1159. https://doi.org/10.1366/0003702055012591.

Frezzotti, M.L., Tecce, F., Casagli, A., 2012. Raman spectroscopy for fluid inclusion analysis. J. Geochem. Explor. 112, 1–20. https://doi.org/10.1016/j.gexplo.2011.09.009.

He, M., Yan, W., Chang, Y., Liu, K., Liu, X., 2019. Fundamental infrared absorption features of α-quartz: an unpolarized single-crystal absorption infrared spectroscopic study. Vib. Spectrosc. 101, 52–63. https://doi.org/10.1016/j.vibspec.2019.02.003.

Izraeli, E.S., Harris, J.W., Navon, O., 2001. Brine inclusions in diamonds: a new upper mantle fluid. Earth Planet Sci. Lett. 187, 323–332. https://doi.org/10.1016/S0012-821X(01)00291-6.

Jain, T.K., Varshney, M., Maitra, A., 1989. Structural studies of aerosol OT reverse micellar aggregates by FT-IR spectroscopy. J. Phys. Chem. 93 (21), 7409–7416. https://doi.org/10.1021/j100358a032.

Jena, K.C., Hore, D.K., 2011. A simple transmission-based approach for determining the thickness of transparent films. Am. J. Phys. 79 (3), 256–260. https://doi.org/10.1119/1.3533710.

Kagi, H., Kiyasu, A., Akagi, T., Nara, M., Sawaki, T., 2006. Near-infrared spectroscopic determination of salinity and internal pressure of fluid inclusions in minerals. Appl. Spectrosc. 60 (4), 430–436. https://doi.org/10.1366/000370206776593735.

Kamiya, Y., Lang, A.R., 1965. On the structure of coated diamonds. Phil. Mag. 11, 347–356. https://doi.org/10.1080/14786436508221861.

Kawamoto, T., Ochiai, S., Kagi, H., 2004. Changes in the structure of water deduced from the pressure dependence of the Raman OH frequency. J. Chem. Phys. 120, 5867–5870. https://doi.org/10.1063/1.1689639.

King, P.L., Ramsey, M.S., McMillan, P.F., Swayze, G., 2004. Laboratory fourier transform infrared spectroscopy methods for geologic samples. In: King, P.L., Ramsey, M.S., Swayze, G. (Eds.), Infrared Spectroscopy in Geochemistry, Exploration Geochemistry, and Remote Sensing. Mineralogical Association of Canada, Ottawa, pp. 57–91.

Konevskikh, T., Ponossov, A., Blümel, R., Lukacs, R., Kohler, A., 2015. Fringes in FTIR spectroscopy revisited: understanding and modelling fringes in infrared spectroscopy of thin films. Analyst 140, 3969–3980. https://doi.org/10.1039/c4an02343a.

Kopylova, M., Navon, O., Dubrovinsky, L., Khachatryan, G., 2010. Carbonatitic mineralogy of natural diamond-forming fluids. Earth Planetary Lett. 291, 126–137. https://doi.org/10.1016/j.epsl.2009.12.056.

Liu, X., Ma, Y., He, Q., He, M., 2017. Some IR features of SiO_4 and OH in coesite, and its amorphization and dehydration at ambient pressure. J. Asian Earth Sci. 148, 315–323. https://doi.org/10.1016/j.jseaes.2017.03.016.

Lu, W., Chou, I.M., Burruss, R.C., 2008. Determination of methane concentrations in water in equilibrium with sI methane hydrate in the absence of a vapor phase by *in situ* Raman spectroscopy. Geochem. Cosmochim. Acta 72, 412–422. https://doi.org/10.1016/j.gca.2007.11.006.

Lu, A., Li, Y., Ding, H., Xu, X., Li, Y., Ren, G., Liang, J., Liu, Y., Hong, H., Chen, N., Chu, S., Liu, F., Li, Y., Wang, H., Ding, C., Wang, C., Lai, Y., Liu, J., Dick, J., Liu, K., Hochella Jr., M.F., 2019. Photoelectric conversion on Earth's surface via widespread Fe- and Mn-mineral coatings. Proc. Natl. Acad. Sci. Unit. States Am. 116 (20), 9741–9746. https://doi.org/10.1073/pnas.1902473116.

Luth, R.W., Stachel, T., 2014. The buffering capacity of lithospheric mantle: implications for diamond formation. Contrib. Mineral. Petrol. 168, 1083. https://doi.org/10.1007/s00410-014-1083-6.

MacDonald, H., Bedwell, B., Gulari, E., 1986. FTIR spectroscopy of microemulsion structure. Am. Chem. Soc. 2, 704–708. https://doi.org/10.1021/la00072a005.

Maley, N., 1992. Critical investigation of the infrared-transmission-data analysis of hydrogenated amorphous silicon alloys. Phys. Rev. B 46 (4), 2078–2085. https://doi.org/10.1103/PhysRevB.46.2078.

Martens, H., Stark, E., 1991. Extended multiplicative signal correction and spectral interference subtraction: new preprocessing methods for near infrared spectroscopy. J. Pharmaceut. Biomed. Anal. 9 (8), 625–635. https://doi.org/10.1016/0731-7085(91)80188-F.

Moritz, H., 1999. Messung des Konzentrationsfeldes verdunstender binärer Mikropartikel mittels linearer Raman-Spektroskopie. Fortschrittsberichte 3. VDI-Verlag, Düsseldorf (in German).

Navon, O., Hutcheon, I.D., Rossman, G.R., Wasserburg, G.J., 1988. Mantle-derived fluids in diamond micro-inclusions. Nature 335 (27), 784–789. https://doi.org/10.1038/335784a0.

Oliver, B.G., Davis, A.R., 1973. Vibrational spectroscopic studies of aqueous alkali metal bicarbonate and carbonate solutions. Can. J. Chem. 51, 698–702. https://doi.org/10.1139/v73-106.

Pasteris, J.D., Wopenka, B., Seitz, J.C., 1988. Practical aspects of quantitative laser Raman microprobe spectroscopy for the study of fluid inclusions. Geochem. Cosmochim. Acta 52, 979–988. https://doi.org/10.1016/0016-7037(88)90253-0.

Perchard, J.P., 2001. Anharmonicity and hydrogen bonding. III. Analysis of the near infrared spectrum of water trapped in argon matrix. Chem. Phys. 273, 217–233. https://doi.org/10.1016/s0301-0104(01)00496-7.

Ratcliffe, C.I., Irish, D.E., 1982. Vibrational spectral studies of solutions at elevated temperatures and pressures. 5. Raman studies of liquid water up to 300 °C. J. Phys. Chem. 86, 4897–4905. https://doi.org/10.1021/j100222a013.

Roedder, E., 1984. Fluid inclusions. In: Ribbe, H.P. (Ed.), Reviews in Mineralogy, vol. 12. Mineralogical Society of America, Washington DC, pp. 1–644.

Roedder, E., 2003. Fluid inclusions. Encycl. Phys. Sci. Technol. 12 (6), 71–77. https://doi.org/10.1016/B0-12-227410-5/00251-9.

Rudolph, W.W., Fischer, D., Irmer, G., 2006. Vibrational spectroscopic studies and density functional theory calculations of speciation in the CO_2-Water system. Appl. Spectrosc. 60 (2), 130–144. https://doi.org/10.1366/000370206776023421.

Rudolph, W.W., Irmer, G., Königsberger, E., 2008. Speciation studies in aqueous HCO_3^--CO_3^{2-} solutions. A combined Raman spectroscopic and thermodynamic study. Dalton Trans. 7 (7), 900–908. https://doi.org/10.1039/b713254a.

Schabel, W., 2005. Inverse mikro-Raman-spektroskopie-eine neue messmethode zur untersuchung lokaler Stofftransportvorgänge in dünnen filmen, folien und membrane. Chem. Ing. Tech. 77 (12), 1915–1926. https://doi.org/10.1002/cite.200500060 (in German).

Schrauder, M., Navon, O., 1994. Hydrous and carbonatitic mantle fluids in fibrous diamonds from Jwaneng, Botswana. Geochem. Cosmochim. Acta 58 (2), 761–771. https://doi.org/10.1016/0016-7037(94)90504-5.

Smart, K.A., Cartigny, P., Tappe, S., O'Brien, H., Klemme, S., 2017. Lithospheric diamond formation as a consequence of methane-rich volatile flooding: an example from diamondiferous eclogite xenoliths of the Karelian craton (Finland). Geochem. Cosmochim. Acta 206, 312–342. https://doi.org/10.1016/j.gca.2017.03.014.

Smith, W.E., Dent, G., 2005. Modern Raman Spectroscopy – A Practical Approach. John Wiley and Sons, Ltd, Chicester, England.

Söhnel, O., Novotny, P., 1985. Densities of Aqueous Solutions of Inorganic Substances. Elsevier, Amsterdam.

Stagno, V., Frost, D.J., 2010. Carbon speciation in the asthenosphere: experimental measurements of the redox conditions at which carbonate-bearing melts coexist with graphite or diamond in peridotite assemblages. Earth Planet Sci. Lett. 300, 72–84. https://doi.org/10.1016/j.epsl.2010.09.038.

Sun, Q., 2009. The Raman OH stretching bands of liquid water. Vib. Spectrosc. 51, 213–217. https://doi.org/10.1016/j.vibspec.2009.05.002.

Sun, Q., Qin, C., 2011. Raman OH stretching band of water as an internal standard to determine carbonate concentrations. Chem. Geol. 283, 274–278. https://doi.org/10.1016/j.chemgeo.2011.01.025.

Sun, Q., Zeng, Y., 2000. Development of in-situ analysis of individual fluid inclusions. Adv. Earth Sci. 15 (6), 673–678. https://doi.org/10.3321/j.issn:1001-8166.2000.06.009 (In Chinese).

Sun, Q., Zhao, L., Li, N., Liu, J., 2010. Raman spectroscopic study for the determination of Cl^- concentration (molarity scale) in aqueous solutions: application to fluid inclusions. Chem. Geol. 272, 55–61. https://doi.org/10.1016/j.chemgeo.2010.02.004.

Sun, Q., Zheng, H., Xu, J., Hines, E., 2003. Raman spectroscopic studies of the stretching band from water up to 6 kbar at 290 K. Chem. Phys. Lett. 379, 427–431. https://doi.org/10.1016/j.cplett.2003.07.028.

Tao, R., Zhang, L., Liu, X., 2015. Oxygen fugacity of Earth's mantle and deep carbon cycle in the subduction zone. Acta Petrol. Sin. 31 (7), 1879–1890 (in Chinese).

Thomas, S.-M., Koch-Müller, M., Reichart, P., Rhede, D., Thomas, R., Wirth, R., Matsyuk, S., 2009. IR calibrations for water determination in olivine, r-GeO_2, and SiO_2 polymorphs. Phys. Chem. Miner. 36, 489–509. https://doi.org/10.1007/s00269-009-0295-1.

Thomas, R., Davidson, P., Schmidt, C., 2011. Extreme alkali bicarbonate- and carbonate-rich fluid inclusions in granite pegmatite from the Precambrian Rønne granite, Bornholm Island, Denmark. Contrib. Mineral. Petrol. 161, 315–329. https://doi.org/10.1007/s00410-010-0533-z.

Tomlinson, E.L., Jones, A.P., Harris, J.W., 2006. Co-existing fluid and silicate inclusions in mantle diamond. Earth Planet Sci. Lett. 250, 581–595. https://doi.org/10.1016/j.epsl.2006.08.005.

Tomlinson, E.L., Müller, W., EIMF, 2009. A snapshot of mantle metasomatism: trace element analysis of coexisting fluid (LA-ICP-MS) and silicate (SIMS) inclusions in fibrous diamonds. Earth Planet Sci. Lett. 279, 362–372. https://doi.org/10.1016/j.epsl.2009.01.010.

Walrafen, G.E., 1964. Raman spectral studies of water structure. J. Chem. Phys. 40 (11), 3249–3256. https://doi.org/10.1063/1.1724992.

Walrafen, G.E., Chu, Y.C., 1995. Linearity between structural correlation length and correlated-proton Raman intensity from amorphous ice and supercooled water up to dense supercritical steam. J. Phys. Chem. 99, 11225–11229. https://doi.org/10.1021/j100028a025.

Wang, X., Hu, W., Chou, I.-M., 2013. Raman spectroscopic characterization on the OH stretching bands in NaCl-Na_2CO_3-Na_2SO_4-CO_2-H_2O systems: implications for the measurement of chloride concentrations in fluid inclusions. J. Geochem. Explor. 132, 111–119. https://doi.org/10.1016/j.gexplo.2013.06.006.

Weng, S., Wu, J., Xu, G., 1985. The fourier transform infrared spectra of liquid water. Fourier Comput. Infrared Spectrosc. 553, 431–432. https://doi.org/10.1117/12.970898.

Wilkinson, J.J., 2001. Fluid inclusions in hydrothermal ore deposits. Lithos 55, 229–272. https://doi.org/10.1016/S0024-4937(00)00047-5.

Wu, J., Zheng, H., 2010. Quantitative measurement of the concentration of sodium carbonate in the system of Na_2CO_3-H_2O by Raman spectroscopy. Chem. Geol. 273, 267–271. https://doi.org/10.1016/j.chemgeo.2010.03.001.

Yamamoto, J., Kagi, H., Kaneoka, I., Lai, Y., Prikhod'ko, V.S., Arai, S., 2002. Fossil pressures of fluid inclusions in mantle xenoliths exhibiting rheology of mantle minerals: implications for the geobarometry of mantle minerals using micro-Raman spectroscopy. Earth Planet Sci. Lett. 198, 511–519. https://doi.org/10.1016/s0012-821x(02)00528-9.

Zhu, Y., Ogasawara, Y., 2002. Carbon recycled into deep Earth: evidence from dolomite dissociation in subduction-zone rocks. Geology 30 (10), 947–950. https://doi.org/10.1130/0091-7613(2002)030<0947:CRIDEE>2.0.CO;2.